Discharge Characteristics under Non-uniform Electric Field in He, Ar and Air at Low Pressures

H. Okubo, S. Yuasa, K. Ota, N. Hayakawa and M. Hikita

Nagoya University, Nagoya, Japan

ABSTRACT

We measured dc discharge inception voltage V_i for various electrode configurations in He, Ar and air in vacuum range from 10^5 to 10^{-1} Pa to determine discharge characteristics under space vacuum environment. By quantitative consideration of the E_i/p distribution in the gap space at the discharge inception, the discharge inception mechanism under nonuniform electric field was investigated in vacuum. At the same time, we observed the discharge profile variation with residual gas pressure and quantitatively analyzed its characteristics, using an image processing technique. Based on the analysis, we found that the dependency of the discharge inception voltage and the length of the discharge path on the residual gas pressure under non-uniform field conditions agreed well with the dependency previously obtained for uniform field conditions.

1. INTRODUCTION

FOR the purpose of energy accumulation, energy storage and distribution, as well as power conditioning to perform many complicated tasks in space stations, reliable electrical insulation technology and HV technology for the space environment are required [1–3].

A space environment has severe and specific characteristics, quite different from those on the ground, in particular, such as the high vacuum, micro gravity, residual gas components, plasma radiation and so on [4]. Even if the gas pressure in high altitude space for satellites and space shuttles *etc.* is in ultra high vacuum, outgassing from the solid dielectric surface may locally increase the pressure to the low or medium vacuum range, resulting in surface discharge and deterioration of the system functions. Thus, investigations of discharge phenomena in low and medium vacuum are important and should be clarified [5–7]. Nevertheless, a few studies have been reported on practical power apparatus with nonuniform electric field in vacuum [8–10, 15].

From the above points of view, we have been investigating discharge phenomena under nonuniform electric field in low and medium vacuum simulating the space environment [11–13]. In this paper, we report on the discharge inception characteristics and the transition of discharge profile under nonuniform electric field in helium (He) and argon (Ar) which are significant components of residual gas in high altitude space. Moreover, we quantified the discharge profile using an image processing technique, to classify the discharge profile under various condition. Work with positive polarity [12] supplements the work reported here.

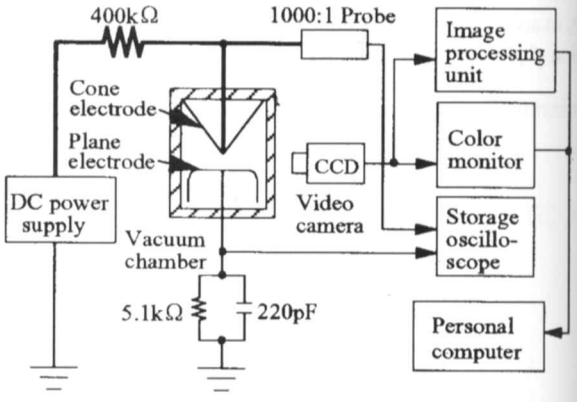

Figure 1. Experimental setup.

	Needle	Rod	Cone	Sphere
Electrode configuration / Gap length g=15mm	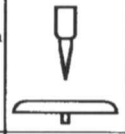		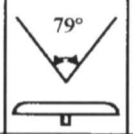	
Tip radius	50μm	1mm	150μm	10mm
NUF	142.2	12.48	5.442	2.224
Material	Stainless steel			

Figure 2. Electrode configurations.

2. EXPERIMENTAL

Figure 1 illustrates the experimental setup composed of a vacuum chamber made of Pyrex™ glass, a dc power supply, a CCD (charge coupled device) video camera, a color monitor and an image processing

1070–9878/97/$3.00

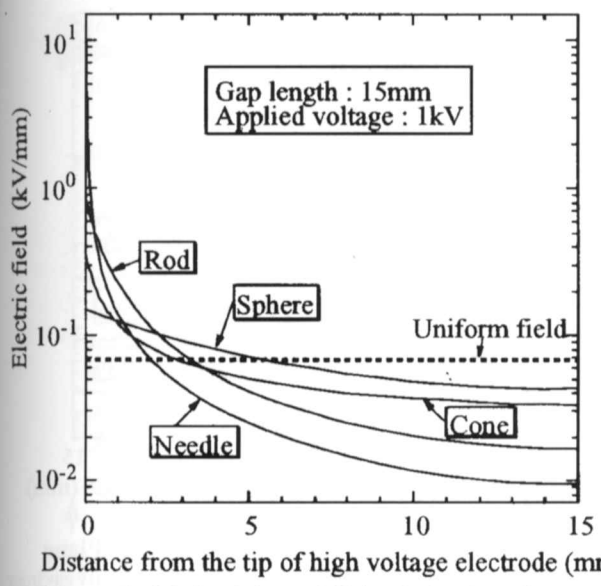

Figure 3. Calculated electric field distribution along the gap.

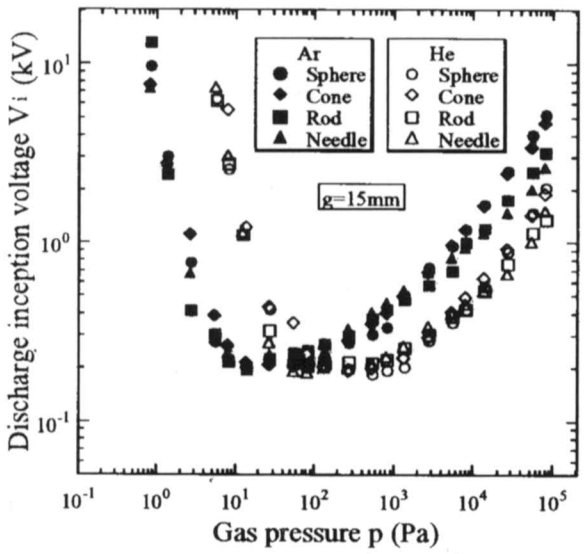

Figure 4. Discharge inception voltage as a function of residual gas pressure in He and Ar for different electrode configurations.

unit. Figure 2 shows the applied electrode configurations. The needle electrode (tip radius of curvature $R = 50$ μm), rod electrode ($R = 1$ mm), cone electrode (head angle 79°, $R = 150$ μm) and sphere electrode ($R = 10$ mm) were placed in the vacuum chamber with a lower plane electrode (165 mm diameter). The electrode configurations form the electric field distributions as shown in Figure 3 with the gap length $g = 15$ mm. The nonuniformity of electric field distribution in the gap space was designated as the factor NUF (non-uniform field): the ratio of the maximum value to the average. At $g = 15$ mm, NUF of needle, rod, cone and sphere to plane electrodes were 142.2, 12.48, 5.442 and 2.224, respectively.

A positive dc ramp voltage was applied to the HV electrode at a rate of 0.1 kV/s. The self-sustaining discharge was detected at higher current levels than 3 μA. Discharge inception voltages were measured by an RC detector with 10 pC sensitivity. Moreover, discharge profiles were observed and recorded with a CCD video camera with available wavelength between 400 and 700 nm. The recorded image data were used for image processing to quantify the discharge shape. The image processing unit has a resolution of 512×512 pixels per image, and one pixel has 256 values of light intensity. All measurements were performed at room temperature.

3. DISCHARGE INCEPTION CHARACTERISTICS IN VACUUM WITH RESIDUAL GASES

3.1. DISCHARG INCEPTION CHARACTERISTICS FOR DIFFERENT ELECTRODE CONFIGURATIONS

Figure 4 shows the pressure p dependence of the discharge inception voltage V_i in He and Ar for different electrode configurations with gap length $g = 15$ mm. The so-called Paschen-like pressure dependence of V_i is seen in the pressure range between 10^5 and 10^{-1} Pa for He and Ar. The values of minimum discharge inception voltages $(V_i)_{min}$ for all electrode configurations are 180 V in He and 220 V in Ar, both of which almost agree with the values of Paschen minimum under uniform field: 150 V in He and 265 V in Ar, respectively [14].

For $p > 1.3 \times 10^3$ Pa, V_i in Ar is 2.5 times higher than that in He. The difference is attributed to the difference of the mean free path of electron between in He and in Ar. Hence, it is quite reasonable that the $V_i - p$ characteristic for Ar shifts to higher voltage on the lower pressure side than that characteristic for He. The vertical trend of the characteristics for He and Ar in the low pressure region rises to higher voltages at much higher pressures than in air [12]. These differences are interpreted in terms of the event that inert gases such as He and Ar easily discharge, due to the long life time of their metastable atoms. On the other hand, in the medium vacuum range, $< 10^2$ Pa, discharge inception characteristics differ from that at $> 10^2$ Pa because of the transition of the discharge path length as will be described in Section 4.

3.2. CRITICAL PRESSURE FOR PD INCEPTION

The discharge was initiated with the form of PD (partial discharge) at $p > 5.3 \times 10^3$ Pa for needle-plane electrodes in He. On the other hand, discharge bridging over the gap occurred without PD at $p \leqslant 5.3 \times 10^3$ Pa even for needle-plane electrodes with the highest field nonuniformity. Let the critical pressure for PD inception be defined as P_C. Figure 5 summarizes P_C in He, Ar and air for different electrode configurations. As seen in Figure 5, P_C depends on the residual gas medium as well as on NUF. We will discuss the discharge inception mechanisms with and without PD in He in the following Section.

3.3. E_i/p DISTRIBUTION IN GAP SPACE

A sufficient number of electrons are needed in the gap space for self-sustaining discharge at the discharge inception, irrespective of the existence of PD. The number of electrons increases in the process of electron avalanche, so that it will be discussed in terms of E_i/p distribution

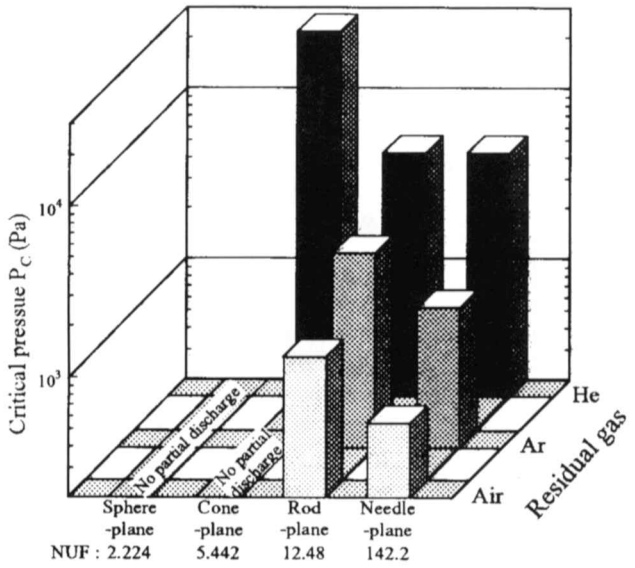

Figure 5. Critical pressure P_C for PD inception for different residual gases.

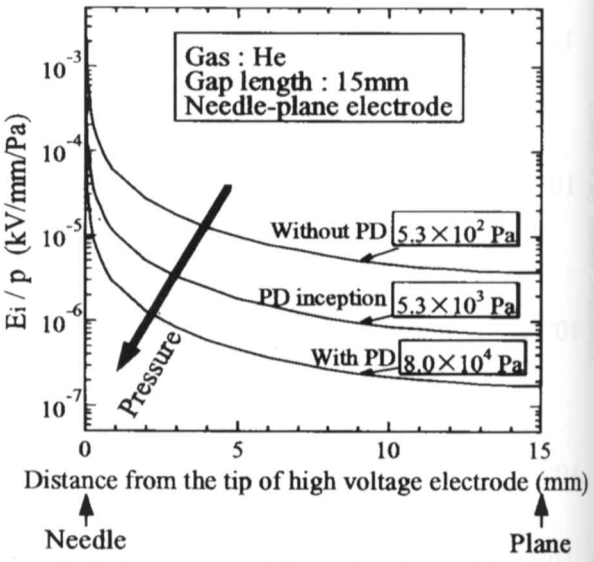

Figure 7. E_i/p as a function of distance from the tip of the HV electrode for needle-plane electrodes.

in the gap space at the discharge inception under nonuniform electric field. From this viewpoint, we discuss the discharge inception mechanism in vacuum by quantitative investigation of the spatial distribution of E_i/p.

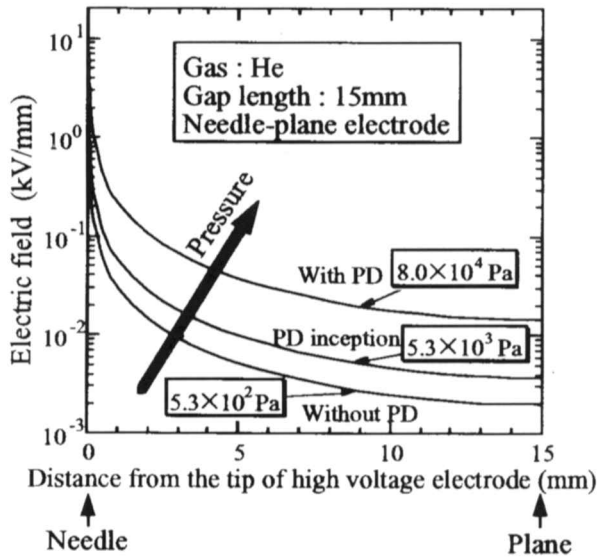

Figure 6. Electric field strength at the discharge inception as a function of distance from the tip of the HV electrode for needle-plane electrodes.

Figure 6 shows the electric field (E_i) distributions in the gap space at the discharge inception for needle-plane electrodes with $g = 15$ mm in He. This Figure indicates E_i distributions at 8.0×10^4 Pa (with PD), 5.3×10^3 Pa (for the critical pressure) and 5.3×10^2 Pa (without PD), respectively. As shown in this Figure, E_i rises with increasing pressure. Figure 7 shows E_i/p distributions obtained by dividing E_i by the corresponding pressure in Figure 6. As shown in this Figure, E_i/p decreases with increasing pressure.

Figure 8 shows the spatial distribution of E_i/p for the cause of PD and discharge bridging over the gap. It is reasonable to assume that there exist a critical level of E_i/p below which effective electron avalanche no longer occurs. This critical level is defined as $(E_i/p)_C$. It is suggested that when E_i/p exceeds $(E_i/p)_C$ partially in the gap space at the discharge inception as shown in Figure 8(a), the number of electrons would increase sufficiently for self-sustaining discharge in the restricted area in the vicinity of the HV electrode, resulting in the PD. On the other hand, as shown in Figure 8(b), discharge over the gap could occur when $E_i/p > (E_i/p)_C$ in the whole gap space at the discharge inception.

If the above mechanism is universal for discharge inception in vacuum, $(E_i/p)_C$ should be independent of the electrode configurations at the critical pressure P_C for PD inception. Figure 9 shows E_i/p distributions at the critical pressure in He for different electrode configurations. As shown in this Figure, $E_i/p > 8.0 \times 10^{-7}$ kV/Pa.mm for each configuration; in other words, $(E_i/p)_C$ in He can be determined as 8.0×10^{-7} kV/Pa.mm irrespective of the electrode configurations. In the same way as the above process in He, $(E_i/p)_C$ in Ar and air can be determined 2.5×10^{-6} kV/Pa.mm and 1.5×10^{-5} kV/Pa.mm, respectively.

As shown above, it was verified that the spatial distribution of E_i/p enables us to classify the discharge inception mechanisms in vacuum into 2 categories with PD and with discharge bridging over the gap. Thus, $(Ei/p)_C$ is expected to be utilized for the insulation design of power apparatus under nonuniform electric field in vacuum.

4. DISCHARGE PROFILES AFTER DISCHARGE INCEPTION

4.1. DISCHARGE PROFILE IN LOW VACUUM

In this Section, we described the discharge profile *i.e.* its shape and locus of light emission, after discharge inception for different residual gas pressures and electric field distributions. Figures 10(a) to (d) show the discharge profile observed in He for cone-plane electrodes with $g =$

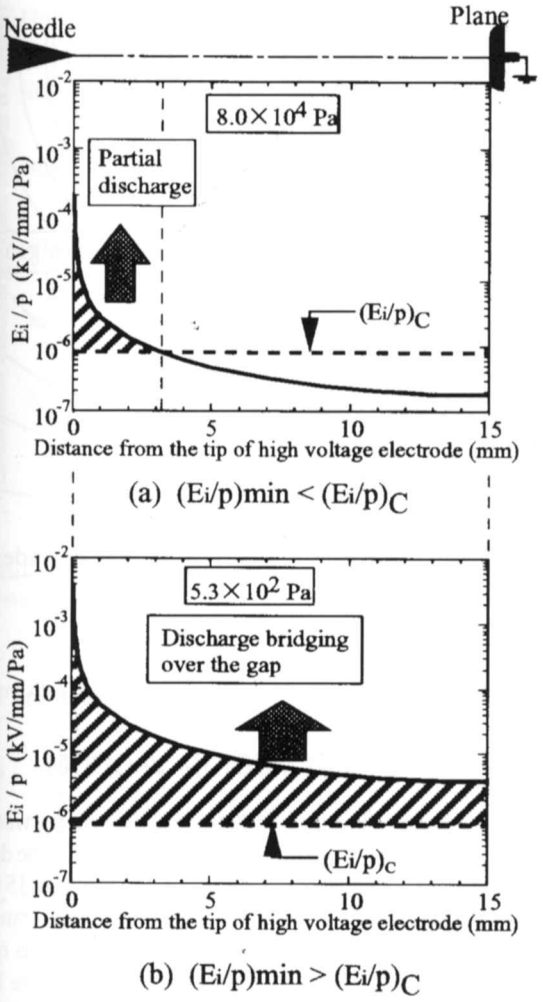

Figure 8. Spatial distribution of E_i/p for PD and discharge bridging over the gap in He.

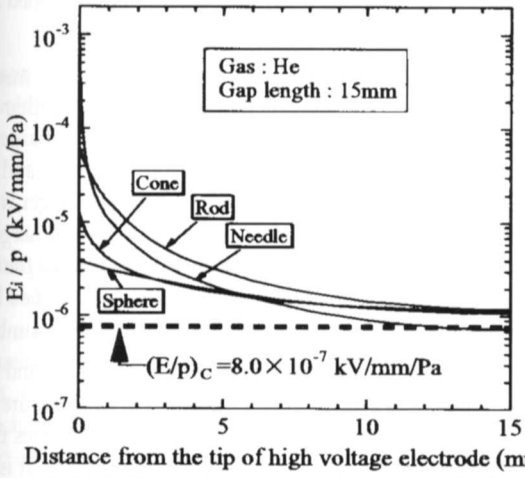

Figure 9. E_i/p distribution at the critical pressure in He for different electrode configurations.

15 mm at different gas pressures: (a) 2.7×10^3 Pa and (b) 530 Pa in the right region of $(V_i)_{min}$ in Figure 4, (c) 270 Pa in the vicinity of $(V_i)_{min}$,

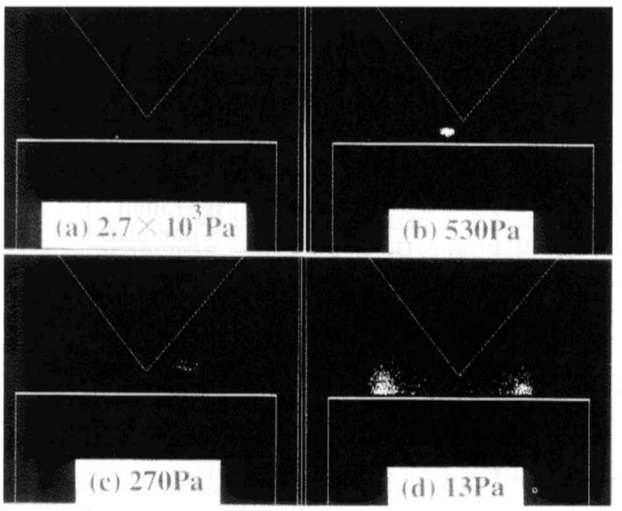

Figure 10. Discharge profile observed in He for cone-plane electrodes with $g = 15$ mm at different residual gas pressures.

(d) 13 Pa in the left region of $(V_i)_{min}$, respectively. These Figures indicate binary images of discharge luminescence using image processing [13]. As shown in Figure 10(a), a small luminous area of negative glow definitely appears in the gap space. The luminous area of negative glow expands and lifts away from the plane electrode at the lower pressure shown in Figure 10(b). With reducing pressure, in Figure 10(c), the negative glow diffuses and is located around the tip of the cone electrode. In Figure 10(d) in the left region of $(V_i)_{min}$, the negative glow disappears and a weak luminous area emerges in the whole chamber. Similar transitions in the discharge profile were observed for the other gases.

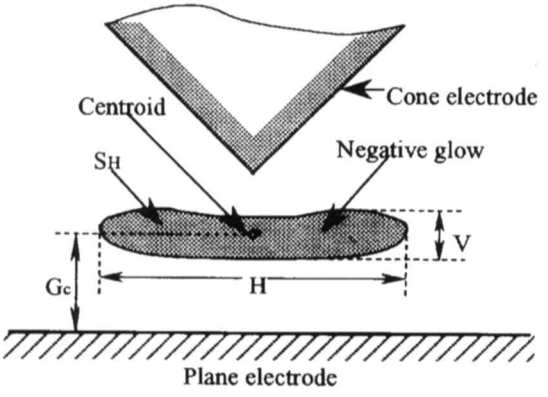

Figure 11. Schematic illustration of shape parameters to characterize the discharge type in the right-hand region of $(V_i)_{min}$.

In the low vacuum in the right region of $(V_i)_{min}$, we introduced 3 shape parameters to characterize the discharge profile: the cross section area S_H of discharge, the flatness rate H/V, and the location G_c of the centroid for negative glow as shown in Figure 11 [13]. Figure 12 shows the cross section area S_H of discharge as a function of gas pressure in He, Ar and air for cone-plane electrodes. As seen in this Figure, S_H rises in the order of air, Ar and He, which corresponds to the order of discharge inception voltage V_i in low vacuum at $p \leqslant 1.3 \times 10^3$ Pa. Figure 13 shows S_H as a function of the mean free path λ_e of electron in He, Ar and air. As shown in this Figure, the λ_e dependence of S_H in He and Ar coincides in the region larger than 1 mm^2 of S_H. This fact

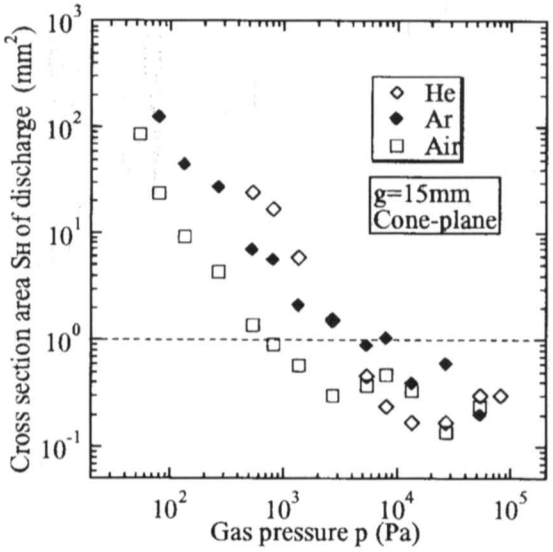

Figure 12. Cross section area S_H of discharge as a function of residual gas pressure in He, Ar and air for cone-plane electrodes.

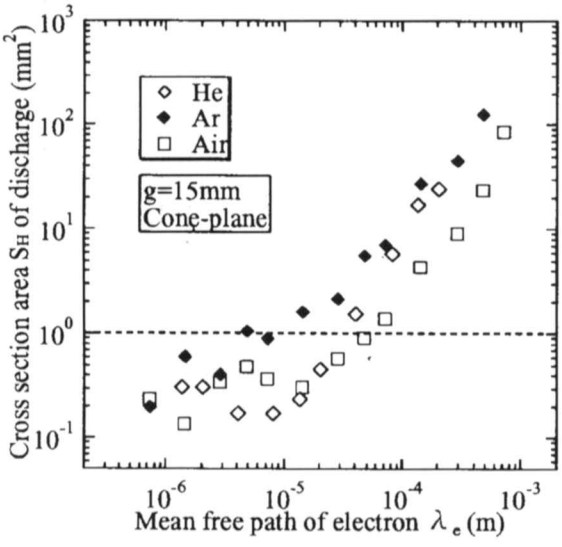

Figure 13. Cross section area S_H of discharge as a function of mean free path λ_e of electrons in He, Ar and air for cone-plane electrodes.

implies that SH in inert gases is standardized by λ_e. On the other hand, S_H in air is rather smaller than those in He and Ar. The difference lies in the gas composition that air consists of diatomic N_2 and electronegative O_2, while He and Ar are inert gases.

Other experiments revealed that the shape parameters were independent of the electrode configuration. These results can be interpreted as follows: the electric field distribution is probably different from the static one before the discharge inception; the maximum electric field emerges between the negative glow and the plane electrode irrespective of electrode configurations. In other words, the electric field distribution with negative glow after the discharge inception depends only on the pressure and gas medium, but not on the electrostatic nonuniformity.

4.2. TRANSITION OF DISCHARGE

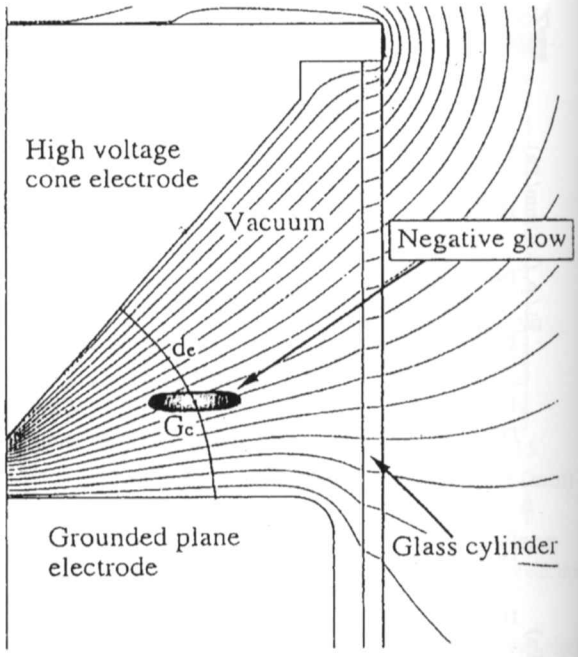

Figure 14. Equipotential lines and estimated discharge path length d_e for cone-plane electrodes.

PATH LENGTH IN MEDIUM VACUUM

As shown in Figure 10(c), the luminous area of discharge was located around the HV electrode in medium vacuum. Specifically, the discharge path length d_e was not equal to the minimum gap length of 15 mm, but larger than the minimum. To clarify the phenomenon, the transition of discharge path length d_e in the medium vacuum range was quantitatively evaluated using the image processing technique. Figure 14 shows the method to get d_e. Firstly, the location G_c of the centroid for negative glow is obtained by image processing. Secondly, the electric line of force passing through G_c is drawn in with the equi-potential lines calculated by the charge simulation method. Finally, d_e is defined as the length of the above electric line of force.

Figure 15 indicates the estimated discharge path length d_e as a function of gas pressure in He and air for cone-plane electrodes with $g = 15$ and 5 mm. As seen in this Figure, in the low vacuum, discharge takes place in the minimum gap between the tip of cone electrode and plane electrode, *i.e.* $d_e = g$. In medium vacuum, d_e becomes longer with reducing pressure. Further decrease of pressure makes the discharge path length at $d_e = 115$ mm corresponding to the length between the upper flange of the chamber and the plane electrode, which is verified by the fact that the weak luminous area is spread over the whole chamber.

Figure 16 shows the discharge inception voltage V_i in He and air for cone-plane electrodes as a function of the product of gas pressure p and estimated discharge path length d_e. In this Figure, solid lines denote Paschen curves for He and air under uniform field [14, 15]. It is obvious in this Figure that V_i under nonuniform electric field agrees well with that under uniform electric field. As with the above methods, we verified experimentally that discharge inception characteristics under nonuniform electric field are similar to those under uniform field, when quantitatively taking into account the transition of the discharge path

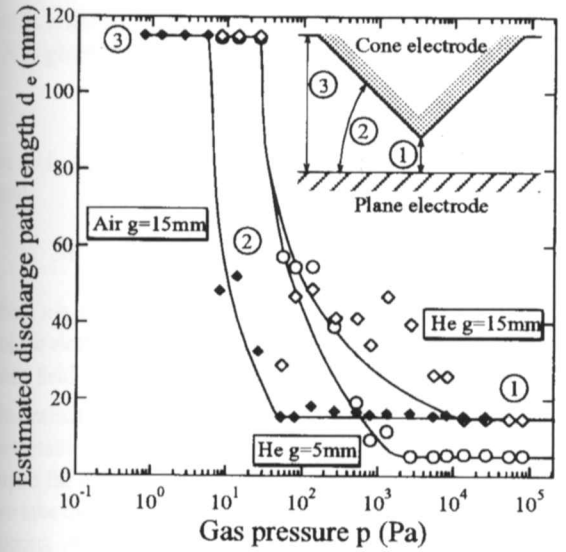

Figure 15. Estimated discharge path length d_e as a function of residual gas pressure in He and air for cone-plane electrodes.

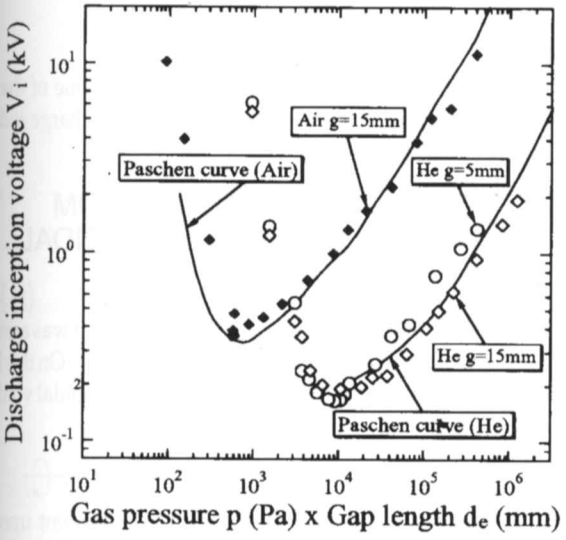

Figure 16. Discharge inception voltage V_i as a function of $(p \times d_e)$ in He and air for cone-plane electrodes.

length.

5. CONCLUSIONS

In this paper, discharge inception characteristics are reported in the low and medium vacuum range of 10^{-1} to 10^5 Pa with residual He, Ar and air under nonuniform electric fields. The discharge inception mechanism in vacuum was classified into 2 categories with and without PD, and also discussed in terms of spatial distribution of E_i/p at the discharge inception. The critical value of E_i/p for PD inception depended on the gas medium, but was independent of the nonuniformity of the electric field.

The discharge profiles after the discharge inception under nonuniform electric field were observed and quantified using an image processing technique. The luminous area of negative glow in low vacuum was related to the mean free path of electrons in He and Ar. Discharge inception under nonuniform and uniform electric fields proved to coincide with each other when considering the pressure dependence of the discharge path length.

REFERENCES

[1] M. Gollor and K. Rogalla, "High Voltage Design of Vacuum Insulated Power Supplies for Space Applications", IEEE Trans. on Elect. Insul., Vol. 28, No. 4, pp. 667–680, 1993.

[2] R. E. Quingley Jr. and L. D. Massie, "Future Trends in Space Power Technology", 26th IECEC, Vol. 2, pp. 1–7, 1991.

[3] L. B. Gordon, "Vacuum Insulation on the Moon", 16th Int. Symp. on Discharges and Electrical Insulation in Vacuum, pp. 459–462, 1994.

[4] M. Lauriente and H. B. Garrett, "A Space Environment Data Resource", Proc. of Spacecraft Charging Technology Conference, p. 556, 1989.

[5] J. M. Meek and J. D. Craggs, *Electrical Breakdown of Gases*, John Wiley & Sons, 1978.

[6] L. B. Loeb, *Basic Processses of Gaseous Electronics*, University of California Press, 1960.

[7] M. Komatsubara, M. Ishii and E. Tsumura, "Research on Outgas and Light Emission from Electrostatic Discharge on Polymer Films in Vacuum", Trans. IEE of Japan, Vol. 114-A, No. 7/8, pp. 528–534, 1994.

[8] W. T. Starr, "High-Altitude Flashover and Corona Problems", Part 1, Design Techniques, Electro-Technology Magazine, May, 1962

[9] W. T. Starr, "High-Altitude Flashover and Corona Problems", Part 2, Experimental Data, Electro-Technology Magazine, June, 1962.

[10] G. G. Karady, M. D. Sirkis and L. Liu, "Investigation of High Altitude Corona Initiation Voltage", 7th ISH, 71.08 1990.

[11] H. Okubo, M. Fujimori, S. Yuasa, N. Hayakawa and M. Hikita, "Image Processing Analysis of Discharge Phenomena under Non-uniform Electric Field in Vacuum", 16th Int. Symp. on Discharges and Electrical Insulation in Vacuum, pp. 372–377, 1994.

[12] N. Hayakawa, M. Fujimori, M. Hikita and H. Okubo, "Analysis of Discharge Phenomena under Non-uniform Electric Field in Vacuum Using Image Processing", IEEE Int. Symp. on Elect. Insul., pp. 241–244, Pittsburgh, 1994.

[13] M. Hikita, M. Fujimori, N. Hayakawa and H. Okubo, "Image Process Discharge Classification under Nonuniform Fields in Air and He at Low Pressure", IEEE Trans. on Dielectrics and Elect. Insul., Vol. 2, No. 2, pp. 263–268, 1995.

[14] A. von Engel, "Ionized Gases", American Institute of Physics, pp. 171–215, 1994.

[15] J. Gerhold and T. W. Dakin, "Paschen Curve for Helium", Electra, No. 52, pp. 80–86, 1977.

Manuscript was received on 11 May 1996, in revised form 23 May 1997.